The International Journal of Advanced Manufacturing Technology (2021) 113:1771–1785
https://doi.org/10.1007/s00170-021-06764-6

ORIGINAL ARTICLE

Influence of anisotropy of KDP crystal on the surface shape deviation of slice by diamond wire saw

Zongqiang Li[1] · Peiqi Ge[1,2] · Wenbo Bi[1,2] · Long Li[1] · Chengyun Li[1]

Received: 27 September 2020 / Accepted: 2 February 2021 / Published online: 13 February 2021

Abstract

KDP crystal is an important functional crystal material used in the fields of laser frequency conversion. Slicing is the first process of KDP crystal processing and the KDP crystal is usually sliced by the diamond wire saw. As KDP crystal is an anisotropic material, the properties of KDP contact with different diamond grits on the diamond wire saw during slicing would be different. The anisotropic properties may lead to the deviation of the diamond wire saw in the thickness direction and form the surface shape deviation of slice. The surface shape deviation would affect the amount of material to be removed and the accuracy of crystal positioning. The commonly used crystal planes of KDP crystal are the (001), the double-frequency, and the triple-frequency crystal plane. In this paper, a model of diamond wire saw considering the anisotropy of KDP crystal is established to obtain the sawing forces, while the anisotropic properties of KDP crystal used in slicing are obtained through coordinate changes. The obtained sawing forces are then applied to the diamond wire saw to obtain the surface shape deviation. Besides, the influence of the tension force on the surface shape deviation is also considered. Based on the established model, the variation rule of surface shape deviation with the feed angle of diamond wire saw is obtained. Results in this paper can reduce the surface shape deviation of slice caused by the anisotropic properties of KDP crystal.

Keywords Anisotropy · Surface shape deviation · KDP crystal · Diamond wire saw · Slicing

Nomenclature

C_l	Length of transverse crack
D	Diameter of the diamond wire saw
D_Z	Deviation of the diamond wire saw in the Z direction
D_{Zmax}	Maximum value of deviation of the diamond wire saw in Z direction
d	Diameter of the diamond grits
d_0	Average diameter of the diamond grits
d_c	Critical depth of KDP crystal
d_{Zmax}	Maximum value of the surface shape deviation of a slice
E	Elastic modulus of KDP crystal
E_d	Degree of anisotropy
f_n	Normal force on the diamond wire saw
f_{nX}	Component of the normal force in the X direction
f_{nY}	Component of the normal force in the Y direction
f_{nZ}	Component of the normal force in the Z direction
f_t	Tangential force of a single diamond grits
H	Hardness of KDP crystal
h_c	Depth of transverse cracks
h_{max}	Largest protrusion height
h_{ij}	Cutting depth of the diamond grit
h_l	Depth of plastic deformation zone
K_c	Fracture toughness of KDP crystal
l	Contact length between the diamond wire saw and KDP crystal
l_1	Length of the diamond wire saw between the two guide wheels
l_2	Length of the diamond wire saw contacts with KDP crystal
P	Nominal load of indentation
s	Feed distance of diamond wire saw
s_{ij}	Flexibility coefficient of KDP crystal
T	Tension force in the diamond wire saw
v_f	Feed speed of KDP crystal

✉ Peiqi Ge
pqge@sdu.edu.cn

[1] School of Mechanical Engineering, Shandong University, Jinan 250061, China

[2] Key Laboratory of High-Efficiency and Clean Mechanical Manufacture, Shandong University, Ministry of Education, Jinan 250061, China

v_s	Move speed of the diamond wire saw
α_0	Cosine value of the crystal direction and the X axis
α_1	A constant to calculate the depth of transverse cracks
β_0	Cosine value of the crystal direction and the Y axis
γ_0	Cosine value of the crystal direction and the Z axis
γ	Feed angle of the diamond wire saw
γ_1	Feed angle of the diamond wire saw of (001) crystal plane
γ_2	Feed angle of the diamond wire saw of the double-frequency crystal plane
γ_3	Feed angle of the diamond wire saw of the triple-frequency crystal plane
η	Density of diamond grits on the surface of diamond wire saw
θ_{ij}	Half vertex angle of the diamond grit
θ_L	Location angle of diamond in the section of diamond wire saw
ξ	A constant to calculate the critical depth of cut
σ	Standard deviation of the size of diamond grit
[hkl]	A crystal orientation in the crystal

1 Introduction

KDP (KH_2PO_4, potassium dihydrogen phosphate) crystal is an important functional crystal material. As its properties of large laser damage threshold [1], KDP crystal is widely used in the fields of laser frequency conversion and photoelectric switch [2]. Slicing is the first process of machining [3]. KDP crystal would be sliced to slices by the diamond wire saw [4, 5]. Schematic of KDP crystal sliced by the diamond wire saw is illustrated in Fig. 1.

It can be observed in Fig. 1 that the diamond wire saw moves in the *Y* direction, while the feed direction of KDP crystal is against the *X* direction.

As KDP crystal is an anisotropic material, properties with different crystal orientation would be very different. The KDP crystal contacts with the diamond wire saw in slicing process would have different crystal orientation and properties. The anisotropic properties of KDP crystal would lead to the deviation of the diamond wire saw in the thickness direction and form the surface shape deviation of the slice.

The slices should meet specific crystal orientation requirements. The (001) crystal plane, the double-frequency crystal plane, and the triple-frequency crystal plane are the crystal planes that should be processed of KDP crystal. All the three crystal planes have precise requirements for crystal orientation. The surface shape deviation caused by the anisotropic properties of KDP crystal would affect the positioning accuracy of the slices. Besides, the surface shape deviation of the slices would determine the amount of material to be removed in subsequent processes and thus affects the material utilization rate. So the effect of anisotropy on surface shape deviation in diamond wire saw slicing of KDP crystal should be investigated.

The anisotropic properties of KDP crystal have been studied by many scholars. Fang [6] studied the mechanical parameters of KDP crystals under several different conditions. Zhang [7] measured the elastic modules of two different crystal planes of KDP crystal by the uniaxial compression test. Guin [8] studied the plastic strain of different crystal planes of KDP crystal by the method of indentation.

In the area of the influence of the anisotropy of KDP crystals on processing, Chen [9] conducted an experimental study on the influence of crystal orientation of KDP crystal on cutting force and machining quality in the single point diamond turning. To explore the anisotropic properties and deformation mechanisms of KDP crystal at the atomic scale, Yang [10] established a potential function for the molecular dynamics (MD) simulations and found that the deformation mechanisms would be affected by the anisotropy.

To study the effect of anisotropy on surface shape deviation in diamond wire saw slicing of KDP crystal, the sawing force on the diamond wire saw needs to be studied. The sawing force has been studied by many researchers by methods of

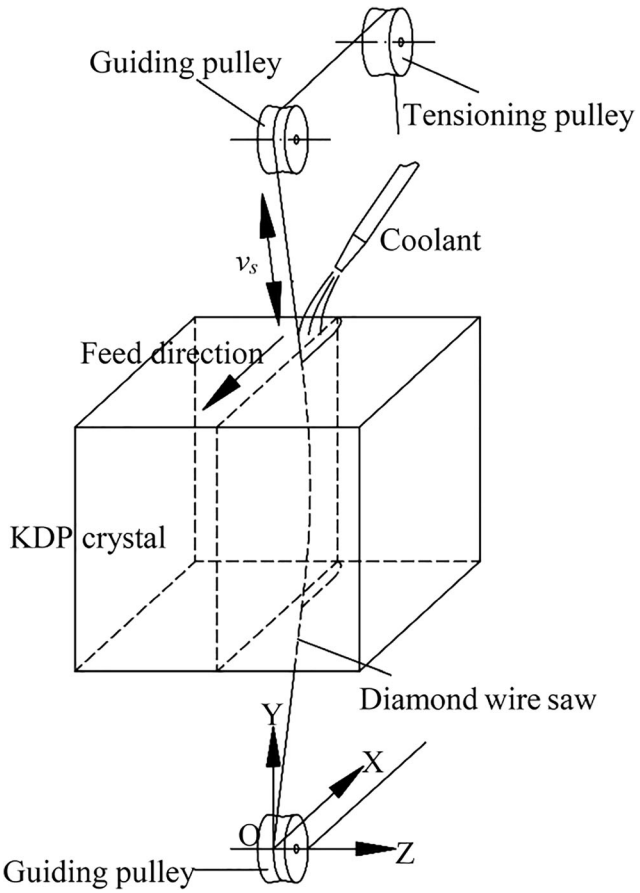

Fig. 1 Schematic of KDP crystal sliced by diamond wire saw

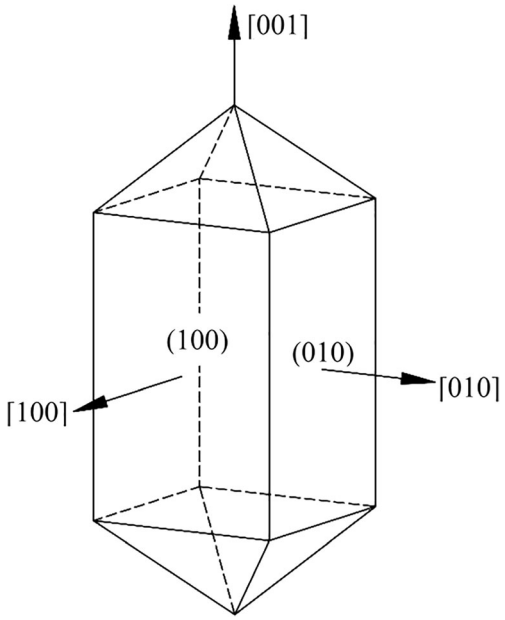

Fig. 2 Ideal outline drawing of KDP crystal

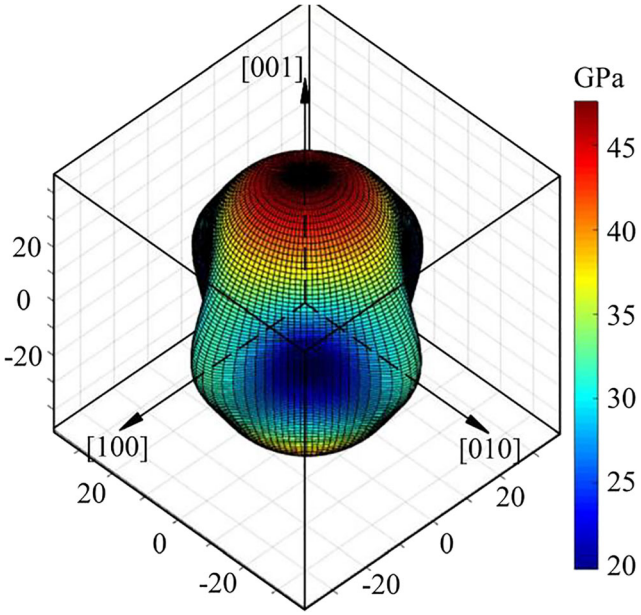

Fig. 3 Distribution of elastic modulus with crystal orientation

experimental measurements and simulation. Clark [11, 12] measured the sawing force of diamond wire saw and studied the force ratio of wood and foam ceramics. The sawing force of SiC [13, 14] is also measured by some researchers. Liu [15] simulated the sawing force of silicon by the diamond wire saw. Wang [16] simulated the sawing force for silicon carbide with the abrasive diamond wire saw. But none of them considered the influence anisotropy to the sawing force. Huang [17] measured the sawing forces of two different crystal planes of sapphire in slicing by the diamond wire saw and found that the forces were different. Though the anisotropy properties of KDP crystals and the influence of anisotropy on processing have been partially studied, the influence of anisotropy on slicing process has not been studied yet.

In this paper, influence of anisotropy of KDP crystal on the surface shape deviation of the slice by the diamond wire saw is studied. The (001) crystal plane, the double-frequency crystal plane, and the triple-frequency crystal plane are studied, respectively, in this paper.

As the anisotropic properties of KDP crystal are determined by the crystal orientation, crystal orientation expressions of KDP crystal in slicing of the three crystal planes with different feed angles of diamond wire saw are studied through coordinate transformation. Then a model of diamond wire saw considering the anisotropic properties of KDP crystals is established. And the sawing forces of the diamond wire saw during slicing are obtained by the model. Finally, the surface shape deviation is obtained by applying sawing forces to the diamond wire saw in ABAQUS.

In this paper, for the (001) crystal plane, the double-frequency crystal plane, and the triple-frequency crystal plane, variation rules of surface shape deviation of slice with the feed angle of diamond wire saw are obtained. Also, change rule of surface shape deviation with the tension is also obtained.

According to the results in this paper, the surface shape deviation of slice caused by anisotropy of KDP crystal can be reduced by selecting appropriate feed angles of diamond wire saw.

Table 1 Flexibility coefficient of KDP crystal

Flexibility coefficient s_{ij}/GPa^{-1}					
s_{11}	s_{12}	s_{13}	s_{33}	s_{44}	s_{66}
0.0311	−0.013	−0.006	0.021	0.079	0.165

2 Anisotropy of KDP crystal in slicing by diamond wire saw

To study the influence of anisotropy on the diamond wire saw slicing, the material properties of the KDP crystal that interacts with the diamond wire saw during slicing should be determined. Anisotropic properties of KDP crystals mainly include elastic modulus, hardness, and critical depth of cut. The elastic modulus of the KDP crystal can be obtained according to its crystal orientation expressions.

The KDP crystal has a tetragonal structure at room temperature. It has a fourth-order symmetry axis and a second-order symmetry axis perpendicular to it. The ideal outline drawing of KDP crystal is shown in Fig. 2.

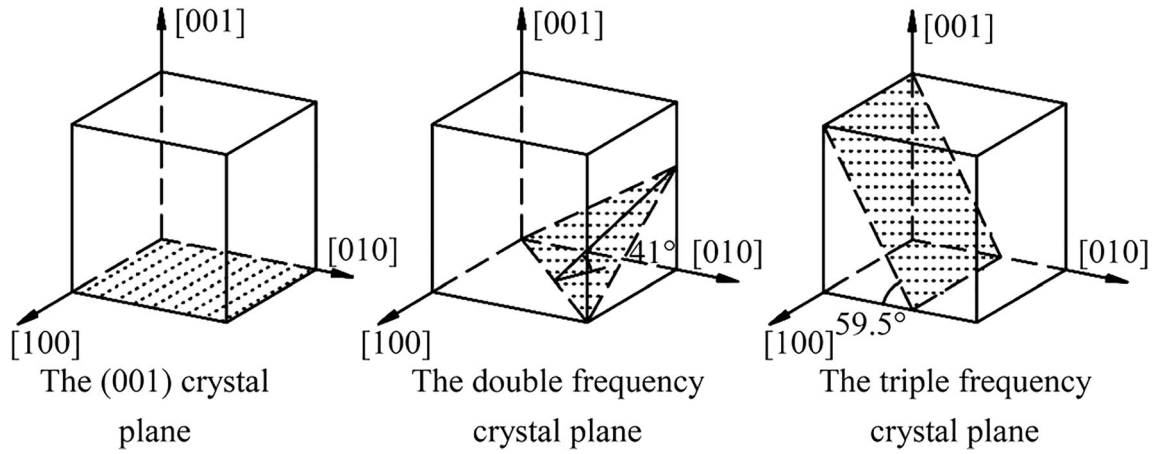

Fig. 4 Schematic of the three crystal planes of KDP crystal

Because of the symmetry of the crystal structure, the elastic modulus corresponding to any crystal direction of the KDP crystal can be obtained by Eq. (1) based on the theory of elasticity.

$$E = 1/\left(s_{11}\left(\alpha_0^4+\beta_0^4\right)+s_{33}\gamma_0^4+(2s_{13}+s_{44})\left(\alpha_0^2+\beta_0^2\right)\gamma_0^2+(2s_{12}+s_{66})\alpha_0^2\beta_0^2\right)$$
$$\text{While,}\begin{cases}\alpha_0 = h/\left(h^2+k^2+l^2\right)\\ \beta_0 = k/\left(h^2+k^2+l^2\right)\\ \gamma_0 = l/\left(h^2+k^2+l^2\right)\end{cases} \tag{1}$$

In Eq. (1), s_{ij} is the flexibility constant of KDP crystal. [*hkl*] is the expression of crystal orientation. While α_0 is the cosine value of the crystal direction and the X axis, β_0 is the cosine value of the crystal direction and the Y axis, and γ_0 is the cosine value of the crystal direction and the Z axis. The flexibility coefficient of KDP crystal is listed in Table 1 [18].

According to Eq. (1), the elastic modulus of any crystal orientation can be calculated as long as the expression of the crystal orientation is determined. Then, distribution of elastic modulus with crystal orientation for KDP crystal can be obtained as shown in Fig. 3.

Therefore, to get the required elastic modulus of KDP crystal used in slicing, expression of the crystal orientation should be determined.

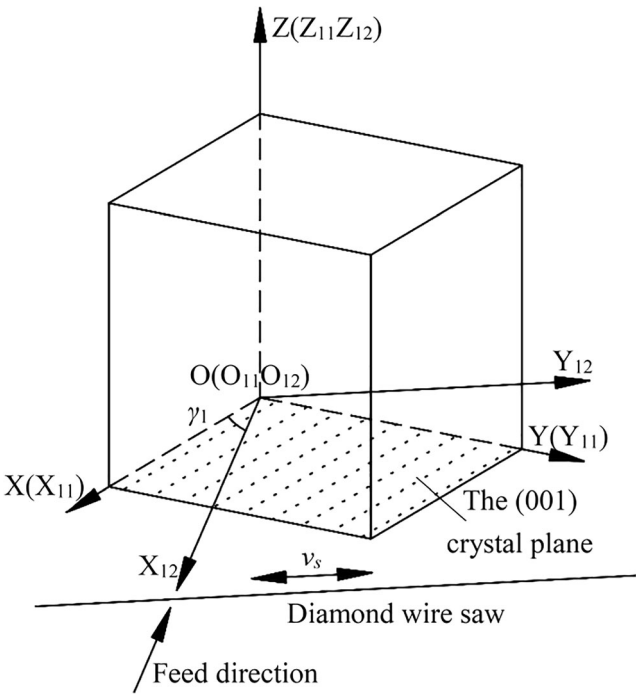

Fig. 5 Schematic of (001) crystal plane conversion

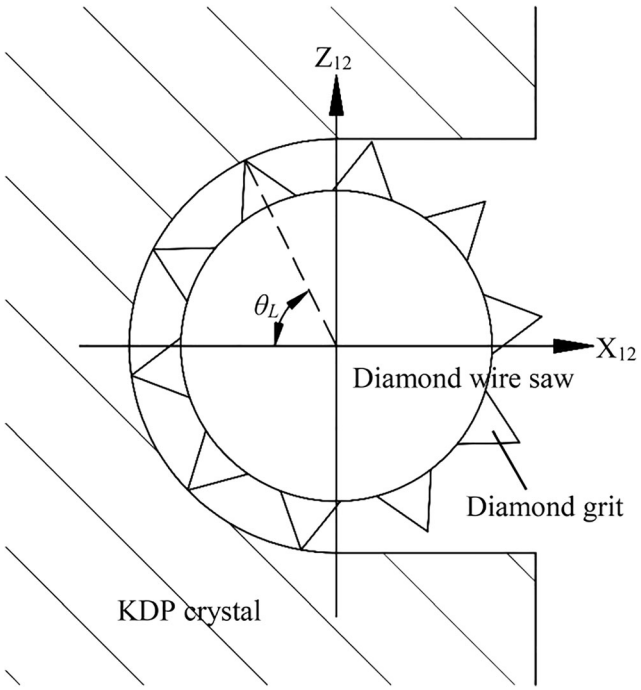

Fig. 6 Distribution of diamond grits on the section of diamond wire saw

2.1 The angular relationship of the three crystal planes

The (001) crystal plane, the double-frequency crystal plane, and the triple-frequency crystal plane are the three commonly used crystal planes of KDP crystal. The schematic of the three crystal planes is shown in Fig. 4.

The (001) crystal plane is the plane perpendicular to the [001] axis. According to the geometric relationship, the double-frequency crystal plane can be obtained by rotating the (001) crystal plane around the [100] axis by 41° and then rotating this plane around the [001] axis by 45°. The triple-frequency crystal plane can be obtained by rotating the (001) crystal plane around the [100] axis by − 59.5°.

2.2 Derivation of coordinate change of the (001) crystal plane

The schematic of coordinate system conversion of the (001) crystal plane during slicing is shown in Fig. 5.

In Fig. 5, the coordinate system of the KDP crystal is OXYZ, while $O_{11}X_{11}Y_{11}Z_{11}$ is the coordinate system of the (001) crystal plane. The initial feed direction of the diamond wire saw is $X_{11}O_{11}$. The angle γ_1 is the feed angle of the diamond wire saw for the (001) crystal plane with the range of 0°–360°.

The change matrix from the coordinate system OXYZ to the (001) crystal plane coordinate system $O_{11}X_{11}Y_{11}Z_{11}$ is $\boldsymbol{T}_{11}$. The coordinate system $O_{12}X_{12}Y_{12}Z_{12}$ can be obtained by rotating the coordinate system $O_{11}X_{11}Y_{11}Z_{11}$ along the Z_{11} axis by the angle γ_1, and its change matrix is $\boldsymbol{T}_{12}$. $\boldsymbol{T}_{11}$ and $\boldsymbol{T}_{12}$ can be deduced by the matrix transformation according to the geometric relationship.

$$T_{11} = \begin{bmatrix} 1\,0\,0 \\ 0\,1\,0 \\ 0\,0\,1 \end{bmatrix} \tag{2}$$

$$T_{12} = \begin{bmatrix} \cos\gamma_1 & -\sin\gamma_1 & 0 \\ \sin\gamma_1 & \cos\gamma_1 & 0 \\ 0 & 0 & 1 \end{bmatrix} \tag{3}$$

To study the effect of anisotropy, elastic modulus at the contact position of the KDP crystal and the diamond wire saw in slicing need to be obtained. Distribution of diamond grits on the section of the diamond wire saw is shown in Fig. 6.

In Fig. 6, the KDP crystal feeds in the X_{12} axis, and the movement direction of the diamond wire saw is the Y_{12} axis, while θ_L is the location angle of the diamond grits on the section of diamond wire saw, whose range is − 90° to 90°. In the coordinate system $O_{12}X_{12}Y_{12}Z_{12}$, expression of the crystal orientation corresponding to the diamond grits with a position angle of θ_L is shown in Eq. (4).

$$A_{12} = \begin{bmatrix} -\cos\theta_L \\ 0 \\ \sin\theta_L \end{bmatrix} \tag{4}$$

$\boldsymbol{A}_1$ is the expression of the crystal orientation in coordinate system OXYZ. It can be obtained by matrix transformation as Eq. (5).

$$A_1 = T_{12}T_{11}A_{12} = \begin{bmatrix} -\cos\gamma_1\cos\theta_L \\ -\sin\gamma_1\cos\theta_L \\ \sin\theta_L \end{bmatrix} \tag{5}$$

By substituting Eq. (5) into Eq. (1), elastic modulus of KDP crystal in slicing of (001) crystal plane can be obtained in Eq. (6).

$$E = 1/\Big(s_{11}(\cos^4\gamma_1 + \sin^4\gamma_1)\cos^4\theta_L + s_{33}\sin^4\theta_L + (2s_{13} + s_{44})\cos^2\theta_L\sin^2\theta_L + (2s_{12} + s_{66})\cos^2\gamma_1\sin^2\gamma_1\cos^4\theta_L\Big) \tag{6}$$

2.3 Derivation of coordinate change of the double-frequency crystal plane

The schematic of coordinate system conversion of the double-frequency crystal plane during slicing is shown in Fig. 7.

In Fig. 7, the coordinate system of the KDP crystal is OXYZ, while $O_{21}X_{21}Y_{21}Z_{21}$ is the coordinate system of the double-frequency crystal plane. The initial feed direction of the diamond wire saw is $X_{21}O_{21}$. The angle γ_2 is the feed angle of the diamond wire saw for the double-frequency

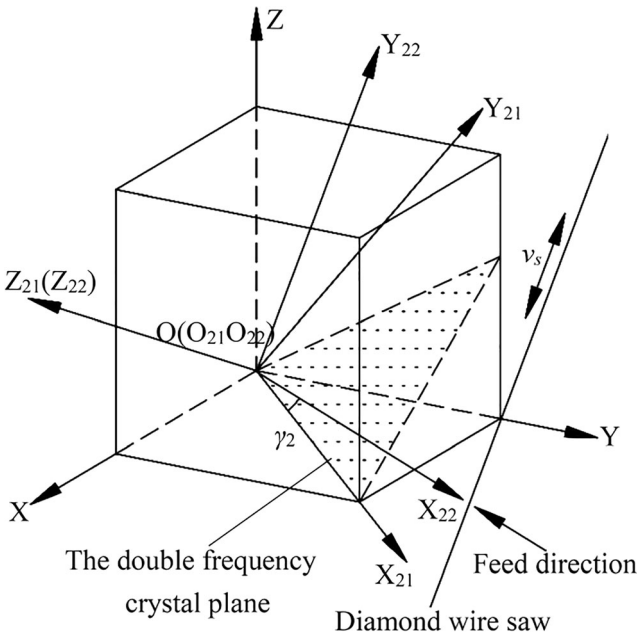

Fig. 7 Schematic of the double-frequency crystal plane conversion

crystal plane with the range of 0°–360°. While the feed angle of the diamond wire saw is γ_2, the coordinate system $O_{22}X_{22}Y_{22}Z_{22}$ can be obtained by rotating $O_{21}X_{21}Y_{21}Z_{21}$ around $O_{21}Z_{21}$ by γ_2.

According to the geometric relationship, the double-frequency crystal plane coordinate system $O_{21}X_{21}Y_{21}Z_2$ is obtained by rotating the coordinate system OXYZ around the X axis by 41° and then rotating it around the Z axis by 45°. The change matrix from the coordinate system OXYZ to $O_{21}X_{21}Y_{21}Z_{21}$ is $\boldsymbol{T}_{21}$.

The coordinate system $O_{22}X_{22}Y_{22}Z_{22}$ is obtained by rotating the coordinate system $O_{21}X_{21}Y_{21}Z_{21}$ around the Z_{21} axis by γ_2, and its change matrix is $\boldsymbol{T}_{22}$. The $\boldsymbol{T}_{21}$ and $\boldsymbol{T}_{22}$ can be deduced by the matrix transformation according to the geometric relationship. The expressions are shown in Eqs. (7) and (8).

$$T_{21} = \begin{bmatrix} \cos45^\circ & -\sin45^\circ\cos41^\circ & \sin45^\circ\sin41^\circ \\ \sin45^\circ & \cos45^\circ\cos41^\circ & -\cos45^\circ\sin41^\circ \\ 0 & \sin41^\circ & \cos41^\circ \end{bmatrix} \tag{7}$$

$$T_{22} = \begin{bmatrix} a_2^2 + (1-a_2^2)\cos\gamma_2 & a_2b_2(1-\cos\gamma_2) - c_2\sin\gamma_2 & a_2c_2(1-\cos\gamma_2) + b_2\sin\gamma_2 \\ a_2b_2(1-\cos\gamma_2) + c_2\sin\gamma_2 & b_2^2 + (1-b_2^2)\cos\gamma_2 & b_2c_2(1-\cos\gamma_2) - a_2\sin\gamma_2 \\ a_2c_2(1-\cos\gamma_2) - b_2\sin\gamma_2 & b_2c_2(1-\cos\gamma_2) + a_2\sin\gamma_2 & c_2^2 + (1-c_2^2)\cos\gamma_2 \end{bmatrix}$$
$$\text{While, } \begin{bmatrix} a_2 \\ b_2 \\ c_2 \end{bmatrix} = \begin{bmatrix} \sin45^\circ\sin41^\circ \\ -\cos45^\circ\sin41^\circ \\ \cos41^\circ \end{bmatrix} \tag{8}$$

Similar to the (001) crystal plane, for the double-frequency crystal plane, expression of the crystal orientation corresponding to the diamond grits with a position angle of θ_L in the coordinate system $O_{22}X_{22}Y_{22}Z_{22}$ is $\boldsymbol{A}_{22}$. Its expression is shown in Eq. (9).

$$A_{22} = \begin{bmatrix} -\cos\theta_L \\ 0 \\ \sin\theta_L \end{bmatrix} \tag{9}$$

$\boldsymbol{A}_2$ is the expression of the crystal orientation in the coordinate system OXYZ. It can be obtained by matrix transformation. Its expression is shown in Eq. (10).

$$A_2 = T_{22}T_{21}A_{22} = \begin{bmatrix} \left(\sqrt{2}/2\right)\left(-\sin\gamma_2\cos\theta_L + (\sin41^\circ\sin\theta_L - \cos41^\circ\cos\gamma_2\cos\theta_L)\right) \\ \left(\sqrt{2}/2\right)\left(-\sin\gamma_2\cos\theta_L - (\sin41^\circ\sin\theta_L - \cos41^\circ\cos\gamma_2\cos\theta_L)\right) \\ \sin41^\circ\cos\gamma_2\cos\theta_L + \cos41^\circ\sin\theta_L \end{bmatrix} \tag{10}$$

Substituting Eq. (10) into Eq. (1), elastic modulus of KDP crystal in slicing of double-frequency crystal plane can be obtained through Eq. (11).

$$E = 1/\left(s_{11}\left(\alpha^4+\beta^4\right) + s_{33}\gamma^4 + (2s_{13}+s_{44})\left(\alpha^2+\beta^2\right)\gamma^2 + (2s_{12}+s_{66})\alpha^2\beta^2\right)$$
$$\text{While, } \begin{cases} \alpha = \left(\sqrt{2}/2\right)\left(-\sin\gamma_2\cos\theta_L + (\sin41^\circ\sin\theta_L - \cos41^\circ\cos\gamma_2\cos\theta_L)\right) \\ \beta = \left(\sqrt{2}/2\right)\left(-\sin\gamma_2\cos\theta_L - (\sin41^\circ\sin\theta_L - \cos41^\circ\cos\gamma_2\cos\theta_L)\right) \\ \gamma = \sin41^\circ\cos\gamma_2\cos\theta_L + \cos41^\circ\sin\theta_L \end{cases} \tag{11}$$

2.4 Derivation of coordinate change of the triple-frequency crystal plane

The schematic of coordinate system conversion of the triple-frequency crystal plane during slicing is shown in Fig. 8.

In Fig. 8, the coordinate system of the KDP crystal is OXYZ, while $O_{31}X_{31}Y_{31}Z_{31}$ is the coordinate system of the triple-frequency crystal plane. The initial feed direction of the diamond wire saw is $X_{31}O_{31}$. The angle γ_3 is the feed angle of the diamond wire saw for the triple-frequency crystal plane with the range of 0°–360°. While the feed angle is γ_3, the coordinate system $O_{32}X_{32}Y_{32}Z_{32}$ can be obtained by rotating $O_{31}X_{31}Y_{31}Z_{31}$ along $O_{31}Z_{31}$ by an angle of γ_3.

According to the geometric relationship, the triple-frequency crystal plane coordinate system $O_{31}X_{31}Y_{31}Z_{31}$ can be obtained by rotating the coordinate system OXYZ around the X axis by − 59.5°. The change matrix from the coordinate system OXYZ to $O_{31}X_{31}Y_{31}Z_{31}$ is $\boldsymbol{T}_{31}$. The coordinate system of $O_{32}X_{32}Y_{32}Z_{32}$ is obtained by rotating the coordinate system $O_{31}X_{31}Y_{31}Z_{31}$ along the $O_{31}Z_{31}$ axis by γ_3, and its change matrix is $\boldsymbol{T}_{32}$. $\boldsymbol{T}_{31}$ and $\boldsymbol{T}_{32}$ can be deduced by the matrix transformation according to the geometric relationship. The expressions are shown in Eqs. (12) and (13).

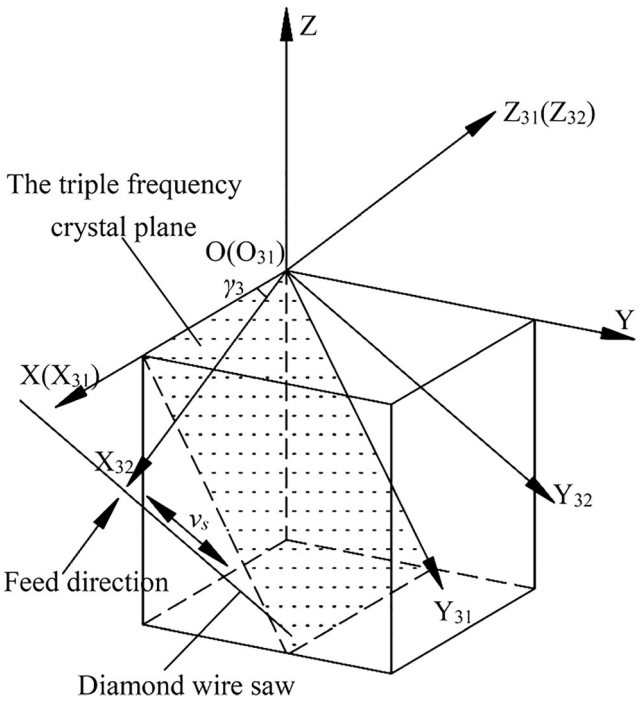

Fig. 8 Schematic of the triple-frequency crystal plane conversion

$$T_{31} = \begin{bmatrix} 1 & 0 & 0 \\ 0 & \cos 59.5^{\circ} & \sin 59.5^{\circ} \\ 0 & -\sin 59.5^{\circ} & \cos 59.5^{\circ} \end{bmatrix} \tag{12}$$

$$T_{32} = \begin{bmatrix} a_3^2 + (1-a_3^2)\cos\gamma_3 & a_3b_3(1-\cos\gamma_3) - c_3\sin\gamma_3 & a_3c_3(1-\cos\gamma_3) + b_3\sin\gamma_3 \\ a_3b_3(1-\cos\gamma_3) + c_3\sin\gamma_3 & b_3^2 + (1-b_3^2)\cos\gamma_3 & b_3c_3(1-\cos\gamma_3) - a_3\sin\gamma_3 \\ a_3c_3(1-\cos\gamma_3) - b_3\sin\gamma_3 & b_3c_3(1-\cos\gamma_3) + a_3\sin\gamma_3 & c_3^2 + (1-c_3^2)\cos\gamma_3 \end{bmatrix}$$
$$\text{While,} \begin{bmatrix} a_3 \\ b_3 \\ c_3 \end{bmatrix} = \begin{bmatrix} 0 \\ \sin 59.5^{\circ} \\ \cos 59.5^{\circ} \end{bmatrix} \tag{13}$$

Similar to the condition of the (001) crystal plane, for the triple-frequency plane, expression of the crystal orientation corresponding to the diamond grits with a position angle of θ_L in the coordinate system $O_{32}X_{32}Y_{32}Z_{32}$ is $\boldsymbol{A}_{32}$. Its expression is shown in Eq. (14).

$$A_{32} = \begin{bmatrix} -\cos\theta_L \\ 0 \\ \sin\theta_L \end{bmatrix} \tag{14}$$

$\boldsymbol{A}_3$ is the expression of the crystal orientation in the coordinate system OXYZ. It can be obtained by matrix transformation. Its expression is shown in Eq. (15).

$$\begin{aligned} A_3 &= T_{32}T_{31}A_{32} \\ &= \begin{bmatrix} -\sin\gamma_3\cos\theta_L \\ \sin 59.5^{\circ}\sin\theta_L + \cos 59.5^{\circ}\cos\theta_L\cos\gamma_3 \\ \cos 59.5^{\circ}\sin\theta_L - \sin 59.5^{\circ}\cos\theta_L\cos\gamma_3 \end{bmatrix} \end{aligned} \tag{15}$$

Substituting Eq. (15) into Eq. (1), the elastic modulus of KDP crystal used in slicing of triple-frequency crystal plane can be obtained through Eq. (16).

$$E = 1/\left(s_{11}\left(\alpha^4 + \beta^4\right) + s_{33}\gamma^4 + (2s_{13} + s_{44})\left(\alpha^2 + \beta^2\right)\gamma^2 + (2s_{12} + s_{66})\alpha^2\beta^2\right)$$
$$\text{While,} \begin{cases} \alpha = -\sin\gamma_3\cos\theta_L \\ \beta = \sin 59.5^{\circ}\sin\theta_L + \cos 59.5^{\circ}\cos\theta_L\cos\gamma_3 \\ \gamma = \cos 59.5^{\circ}\sin\theta_L - \sin 59.5^{\circ}\cos\theta_L\cos\gamma_3 \end{cases} \tag{16}$$

Hardness of KDP crystal in any crystal direction can be obtained from Eq. (17):

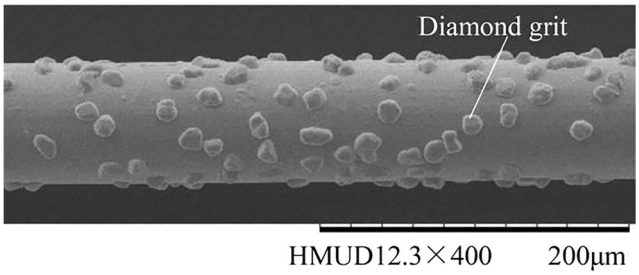

Fig. 9 SEM image of a diamond wire saw

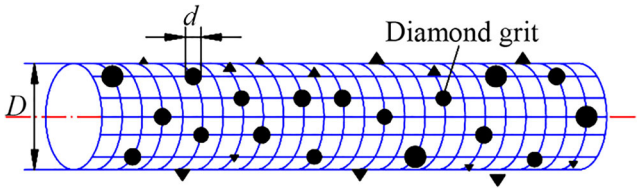

Fig. 10 Schematic of diamond grit distribution on diamond wire saw

$$H = 0.0226E + 0.7555 \tag{17}$$

where H is the hardness of KDP crystal and E is the elastic modulus of KDP crystal.

The fracture toughness of KDP crystal is K_c. It can be obtained by Eq. (18):

$$K_c = k(E/H)^n P/c^{1.5} \tag{18}$$

where k is 0.016, n is 0.5, E is the elastic modulus, H is the hardness, P is the nominal load of indentation, and $P/c^{1.5}$ is a constant value which can be calculated from the known data.

The critical depth of KDP crystal is d_c. It can be obtained by Eq. (19).

$$d_c = \xi(K_c/H)^2(E/H) \tag{19}$$

While ξ is 0.3717, it is a constant that depends on the processing condition.

Therefore, the anisotropic properties of KDP crystal in slicing by the diamond wire saw can be obtained.

3 Simulation of the surface shape deviation

To obtain the surface shape deviation in slicing, the sawing force should be determined firstly. A model of the diamond wire saw is established to calculate the sawing force in the slicing process considering the anisotropic properties of KDP crystal.

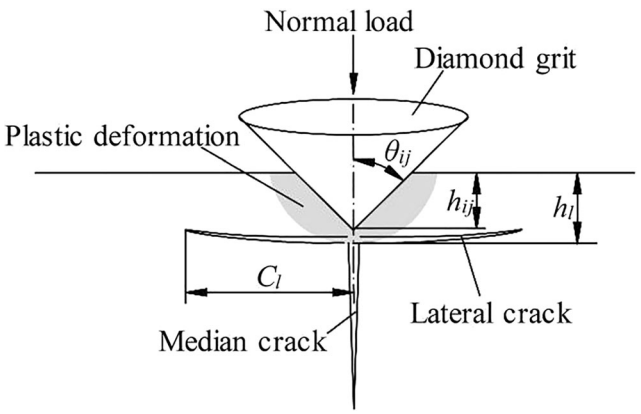

Fig. 11 Schematic of cracks during brittleness removal

3.1 Simulation of the sawing force

3.1.1 Establishing a diamond wire saw model

The SEM image of a diamond wire saw is shown in Fig. 9. A diamond wire saw model is established as Fig. 10.

In Fig. 10, the diameter of the diamond wire saw is D, and the diameter of the diamond grit is d. The density of diamond grit distribution is η. Diamond grits are assumed to be distributed randomly on the diamond wire saw surface and do not overlap each other. The diameter of the diamond grit is normally distributed [19], while the average diameter is d_0, and its standard deviation σ is 3.33. Then the probability of diamond grit with diameter d is in Eq. (20).

$$p(d) = \exp\left(-(d-d_0)^2/(2\sigma^2)\right)/\left(\sqrt{2\pi}\sigma\right) \tag{20}$$

3.1.2 Sawing force and removed material of a single diamond grit

The material removal mechanism of the diamond wire saw is similar to the indentation and scratching. The diamond grits are generally considered as rigid bodies [20]. Diamond grits are usually simplified into the sphere [21, 22] or the cone [15] shape in simulation. According to the observation of the tip morphology of diamond grits [23], the tip of the abrasive particle is mostly triangular pyramid. To simplify the analysis, the shape of the abrasive grains is equivalent to a cone in this paper. Indentation fracture mechanics can be utilized to analyze the force on a single diamond grits from a micro perspective.

Though the mechanism between the diamond grits and the workpiece is complicated, the normal force of a diamond grit can be calculated by Eq. (21) as long as the cutting depth is known [24]:

$$f_{nij} = \pi H h_{ij}^2 \tan^2\theta_{ij}/2 \tag{21}$$

where f_{nij} is the normal force, h_{ij} is the cutting depth, and θ_{ij} is the half vertex angle of diamond grit.

The material removal method depends on the cutting depth of the diamond grit. When the cutting depth is less than the critical cutting depth, the material is removed in the plastic mode. While the cutting depth is larger than the critical cutting depth, the material would be removed in the brittle mode [25]. When the material is removed in brittle mode, the schematic of the cracks is shown in Fig. 11.

In Fig. 11, C_l is the length of lateral crack [26].

$$C_l = \alpha_l\left((\cot\varphi)^{5/6}(E/H)^{3/4}/\left(K_c H^{1/4}\right)\right)^{1/2} P^{5/8} \tag{22}$$

α_l is a constant independent of the indenter and material of workpiece whose value is 0.226.

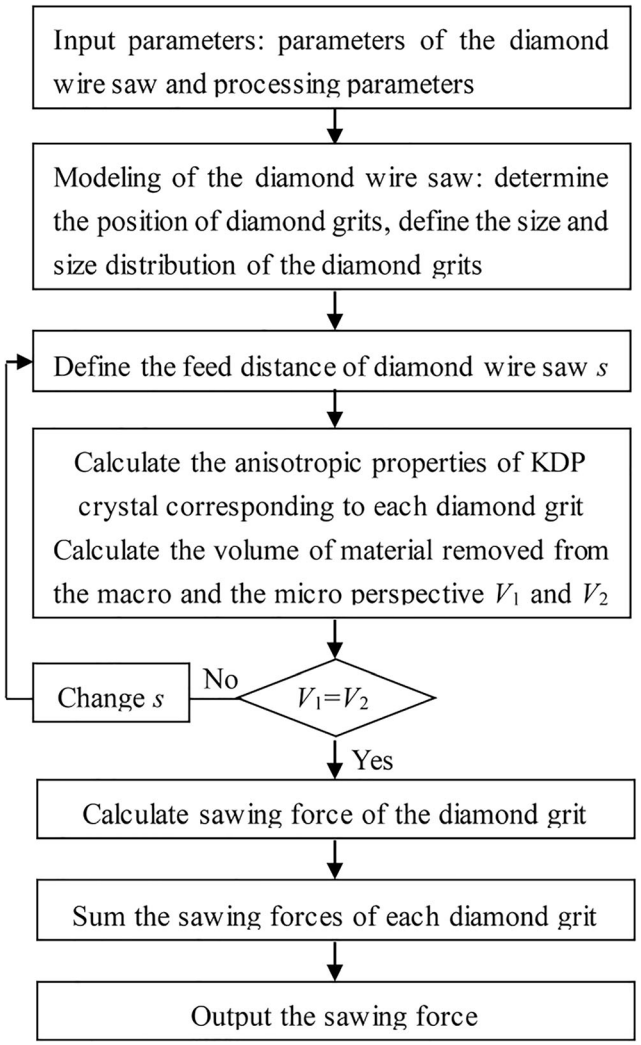

Fig. 12 Process of simulation of the sawing force

The depth of plastic deformation zone can be considered the depth of lateral cracks [27]. It can be obtained by Eq. (23):

$$h_l = \alpha_l(\cot\varphi)^{1/3}E^{1/2}P^{1/2}/H \tag{23}$$

where h_l is the depth of lateral cracks.

According to the research of Chung [28], the tangential force of a diamond grit can be calculated by Eq. (24).

$$f_t = \begin{cases} H_1 h_{ij}^2 \tan\theta_{ij} & (0 < h < d_c) \\ 2H_1 C_l h_l & (d_c \le h < d_c) \end{cases} \tag{24}$$

The feed distance of diamond wire saw is defined as s. It can be obtained by comparing the amount of material removed from the macro and micro perspectives. The cutting depths of the diamond grits can be obtained by Eq. (25) according to the geometric relationship in a diamond wire saw section.

Table 2 Parameters used in the simulation of sawing forces

Parameter	Value
Crystal plane	3 crystal planes
Diameter of the diamond wire saw D/μm	450
Average diameter of diamond grit d/μm	50
Density of diamond grit η/mm^{-1}	83
Length of the diamond wire saw contacts with KDP crystal l_2/mm	300
Feed angle of the diamond wire saw γ/°	0–360

$$h_{ij} = s\cos\theta_{Lij} - \left(d_{\max} - d_{ij}\right) \tag{25}$$

While d_{ij} is the exposed height of the diamond grits, d_{max} is the largest value in the diamond wire saw section.

The material removed by a diamond grit is shown in Eq. (26).

$$V_{ij} = \begin{cases} v_s t h_{ij}^2 \tan\theta_{ij} & \left(h_{ij} < d_c\right) \\ 2 v_s t c_{lij} h_{cij} & \left(h_{ij} \geq d_c\right) \end{cases} \tag{26}$$

From the micro perspective, the total volume removed by the diamond grits can be obtained by Eq. (27).

$$V_1 = \sum V_{ij} \tag{27}$$

From the macro perspective, the volume of material removed within time t is V_2. It can be obtained in Eq. (28):

$$V_2 = D l_2 v_f t \tag{28}$$

where l_2 is the length of the diamond wire saw contacts with KDP crystal.

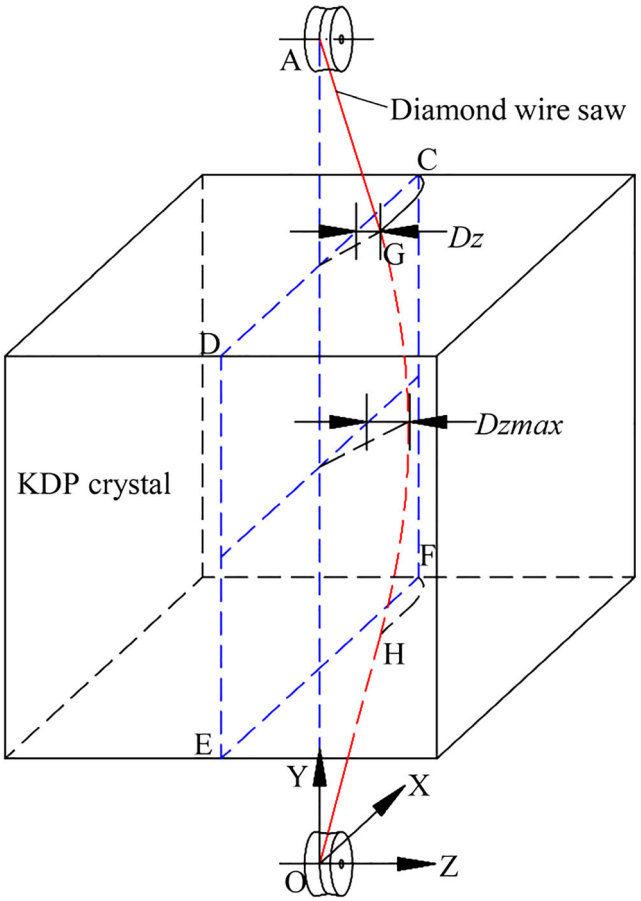

Fig. 13 Schematic of deformation of diamond wire saw in slicing

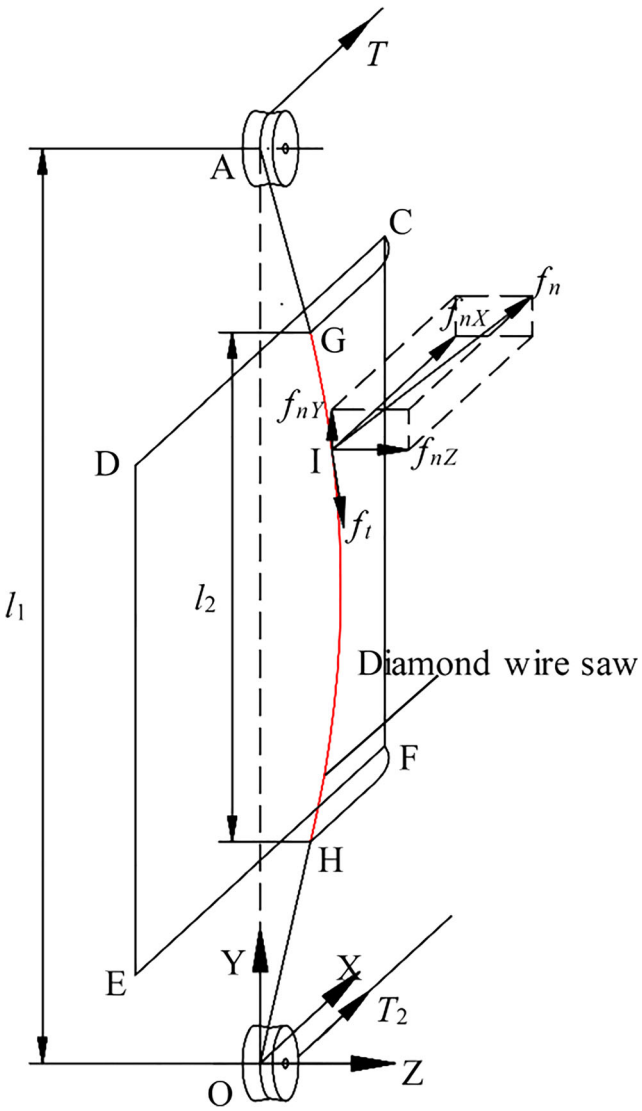

Fig. 14 Schematic of the forces in slicing

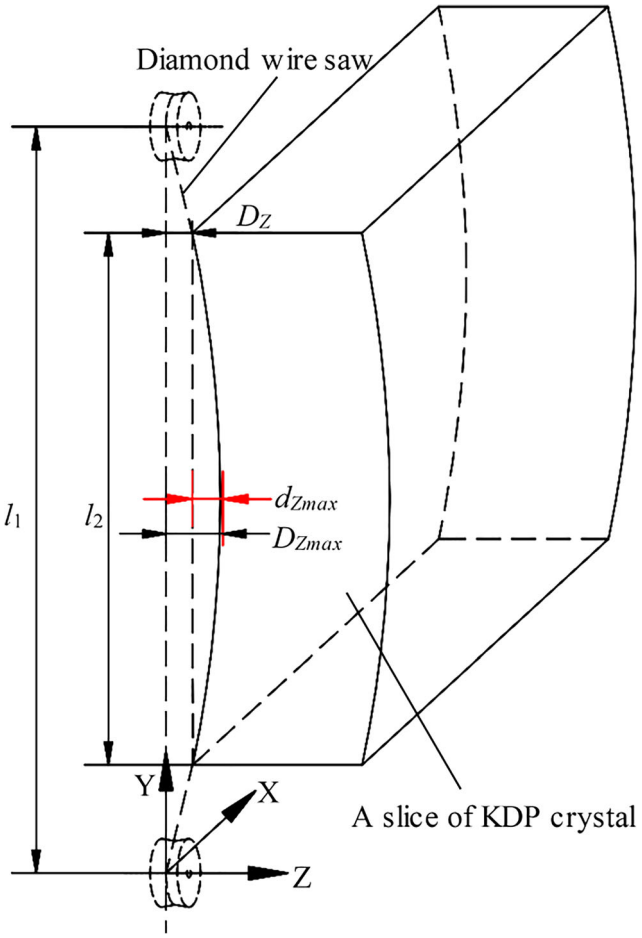

Fig. 15 Schemic of a slice of KDP crystal

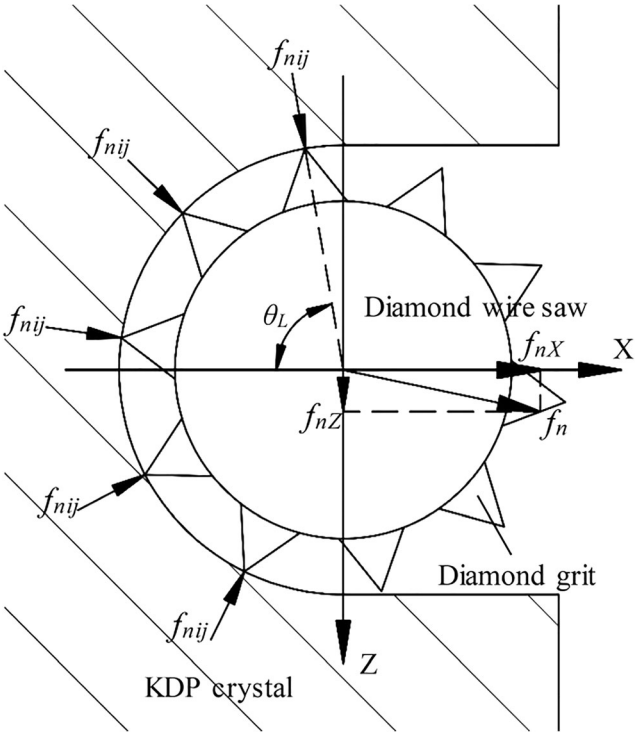

Fig. 16 Schematic of forces on the section of the diamond wire saw

According to Eqs. (27) and (28), s can be obtained by iterative calculation in Matlab. Substituting the obtained s into Eqs. (21) and (24), the sawing forces of the diamond grits can be obtained. The process of simulation of the sawing force is shown in Fig. 12.

Some parameters used in the simulation of sawing force are shown in Table 2.

At last, the sawing forces of the three crystal planes in KDP crystal with different feed angles of the diamond wire saw are got by simulation.

3.2 Calculation of the surface shape deviation

The schematic of deformation of the diamond wire saw in slicing is shown in Fig. 13.

In Fig. 13, the surface *CDEF* is the ideal plane to be formed. The line *AGHB* is the trajectory formed by the diamond wire saw while the diamond wire saw has an offset in the Z direction.

The force analysis of the diamond wire saw in slicing is shown in Fig. 14. The length of the diamond wire saw between the two guide wheels is l_1. While l_2 is the length of the diamond wire saw contacts with KDP crystal, it is the red part in Fig. 14.

In Fig. 14, T and T_2 are tension forces, f_n is the normal force, and f_t is the tangential force. *GH* is a part of the diamond wire saw contacts with the KDP crystal, where the f_n and f_t are distributed. The direction of f_n is perpendicular to the wire. For a point I on *GH*, f_n can be broken down into three component forces f_{nX}, f_{nY}, and f_{nZ} in the X, Y, and Z directions. The direction of f_t is parallel to the axis of the diamond wire saw.

The slice sliced by the diamond wire saw can be obtained by moving the trajectory curve *GH* along the X direction. The schemic of a slice of KDP crystal is shown in Fig. 15.

The diamond wire saw would deform in the Z direction due to the f_{nZ}. As shown in Fig. 15, deviation of the diamond wire saw in the Z direction is recorded as D_Z. In the length of l_1, the maximum deviation of the diamond wire saw in the Z direction is recorded as D_{Zmax}. In the length of l_2, the maximum deviation of the diamond wire saw in the Z direction is recorded as d_{Zmax}. The d_{Zmax} is the maximum value of the surface shape deviation of a slice, and d_{Zmax} is the object that should be studied in this paper.

To obtain the surface shape deviation of slice, the sawing forces are applied to an ABAQUS model to calculate the deformation of the diamond wire saw. After simulation of the deformation of the diamond wire saw is done, the coordinate values of each node on the diamond wire saw are achieved in the post-processing stage. Also, the trajectory expression of the diamond wire saw can be obtained by curve

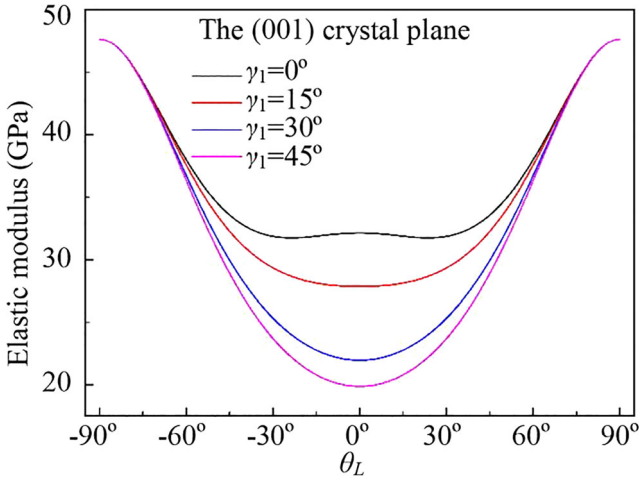

Fig. 17 Variation of E with position angle θ_L for (001) crystal plane

fitting. As a result, the surface shape deviation of slice by diamond wire saw can be obtained.

4 Results and discussion

4.1 Distribution of elastic modulus on the cross section of diamond wire saw

The schematic of the forces on the section of the diamond wire saw during slicing is shown in Fig. 16.

The feed direction of the diamond wire saw is -X. The thickness direction of the slice is the Z axis. The f_{nij} is the normal force of the diamond grit. On the section of the diamond wire saw, the resultant force of f_{nij} is f_n. The component of f_n in the Z direction is f_{nZ}. While the elastic modulus on both sides of the feed direction on the saw wire section is symmetrical, the f_{nZ} would be zero. In this condition, the diamond wire saw would have no deviation in the Z direction. As a result, the anisotropy of KDP crystal would have no influence on the surface shape deviation of the slice.

4.1.1 Distribution of elastic modulus in slicing of the (001) crystal plane

In slicing of the (001) crystal plane with the feed angle γ_1, elastic modulus of KDP crystal can be obtained according to Eq. (6). If the properties of the KDP crystal are symmetric about the feeding direction, Eq. (29) needs to be established.

$$E(\theta_L) = E(-\theta_L) \tag{29}$$

The result can be obtained by substituting Eq. (6) into Eq. (29). It can be noticed that Eq. (29) can be satisfied for all feed angles of (001) crystal plane. In slicing of the (001) crystal plane, variation of the elastic modulus with position angle θ_L can be drawn according to Eq. (6), as shown in Fig. 17.

It can also be noticed from Fig. 17 that the elastic modules are symmetrical about the 0 degree while the feed angle γ_1 has different values. For any feed angle of the diamond wire saw, the elastic modulus in the diamond wire saw section is symmetrical about the feed direction. According to the Neumann principle in crystal physics, the symmetry of crystal physical properties is contained in its microstructure. Once the elastic modulus is symmetrical, other physical properties of the KDP crystal would also be symmetrical.

In conclusion, the anisotropic properties of KDP crystal have no effect on the surface shape deviation of the (001) crystal plane in slicing by the diamond wire saw.

4.1.2 Distribution of elastic modulus in slicing of the double-frequency crystal plane

The elastic modulus of KDP crystal in slicing of the double-frequency plane with the feed angle γ_2 can be obtained according to Eq. (11). If the properties of the KDP crystal are

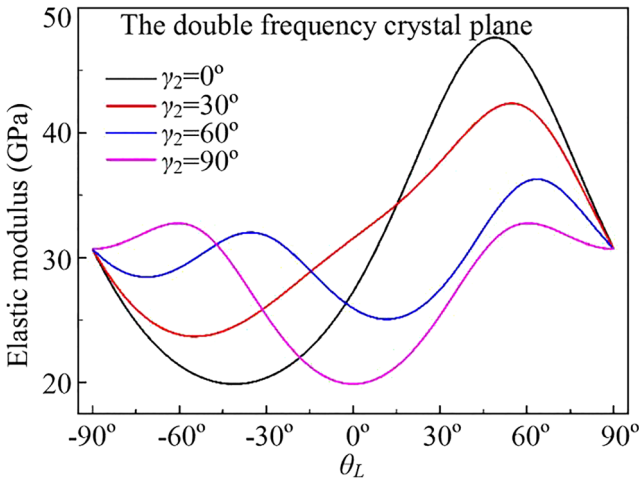

Fig. 18 Variation of E with θ_L for the double-frequency crystal plane

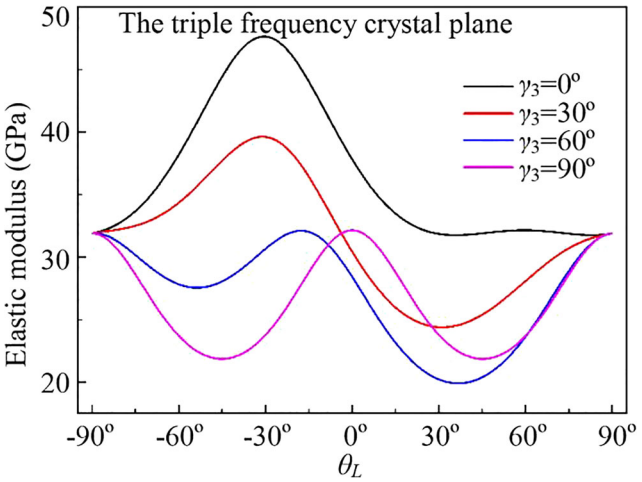

Fig. 19 Variation of E with θ_L for the triple-frequency crystal plane

symmetric about the feeding direction, Eq. (29) needs to be established.

The result can be got by substituting Eq. (11) into Eq. (29) that Eq. (29) can be satisfied while the γ_2 is 90° or 270°.

In slicing of the double-frequency crystal plane, variation of the elastic modulus with position angle θ_L can be drawn according to Eq. (11), as shown in Fig. 18.

It can be seen from Fig. 18 that the distribution of E on the cross section of the diamond wire saw is symmetric about the 0 degree while γ_2 has a value of 90°. The distribution of E would be asymmetric while the γ_2 has other values.

That is to say, anisotropic properties of KDP crystal would affect the surface shape deviation of the double-frequency plane in slicing by the diamond wire saw. The degree of influence would be different while γ_2 has different values.

4.1.3 Distribution of elastic modulus in slicing of the triple-frequency crystal plane

In slicing of the triple-frequency crystal plane with the feed angle γ_3, elastic modulus of KDP crystal can be got according to Eq. (16). If the properties of the KDP crystal are symmetric about the feeding direction, Eq. (29) needs to be established.

The result can be got by substituting Eq. (16) into Eq. (29) that Eq. (29) can be satisfied while γ_3 has values of 90° or 270°.

In slicing of the triple-frequency crystal plane, variation of the elastic modulus with position angle θ_L can be drawn according to Eq. (16), as shown in Fig. 19.

It can be seen from Fig. 19 that the distribution of E on the cross section of the diamond wire saw is symmetric about the 0° while the γ_3 has a value of 90°. The distribution of E would be asymmetric while the γ_3 has other values.

That is to say, the anisotropic properties of KDP crystal would affect the surface shape deviation of the triple-frequency plane in slicing by the diamond wire saw. The degree of influence would be different while γ_3 has different values.

4.1.4 Degree of anisotropic properties of KDP crystal

To study the degree of anisotropic properties of KDP crystal, the f_{nz} needs to be considered. The f_{nz} is a component of the normal force in the Z direction, and it can be got by Eq. (30).

$$f_{nz} = \pi H_1 h_{ij}^2 \left(\tan\theta_{ij}\right)^2 \sin\theta_L / 2 \tag{30}$$

The sine values of the elastic modulus at both sides of the feed direction are integrated respectively, and the difference of the integration results is defined as the degree of anisotropy E_d of the elastic modulus.

$$E_d = \left(\left|\int_{-\pi/2}^{0} E\sin\theta_L d\theta_L\right| - \left|\int_{0}^{\pi/2} E\sin\theta_L d\theta_L\right|\right) \Big/ \left|\int_{-\pi/2}^{\pi/2} E\sin\theta_L d\theta_L\right| \tag{31}$$

As shown in Eq. (31), E_d can be regarded as a degree of anisotropy of the KDP crystal. The E_d is used to characterize the degree of influence of anisotropy on the slice. While E_d has small values, the anisotropy of KDP crystal would have a small effect on the slice and vice versa. According to Eq. (31), variation of E_d with the feed angle of the diamond wire saw of three crystal planes can be obtained, as shown in Fig. 20.

It can be observed from Fig. 20 that, for the (001) crystal plane, the E_d would be zero regardless of the feed angle of the diamond wire saw.

For the double-frequency crystal plane, the E_d would have peak values while the feed angle of diamond wire saw has values of 0° or 180°. While the feed angle is in the range of 60° to 120° and 240° to 300°, the corresponding E_d is close to zero.

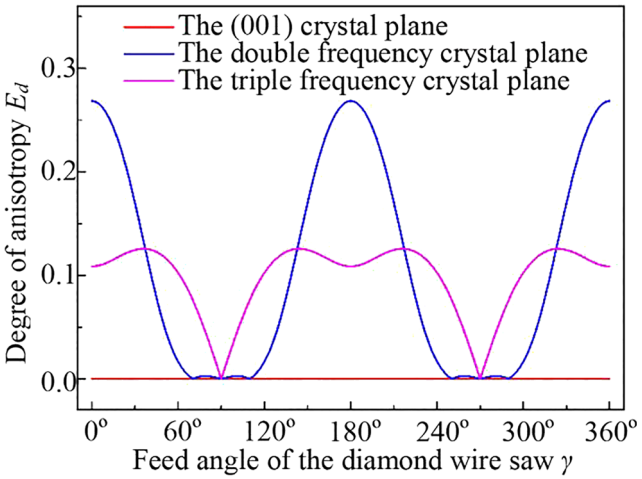

Fig. 20 Variations of E_d with γ of three crystal planes

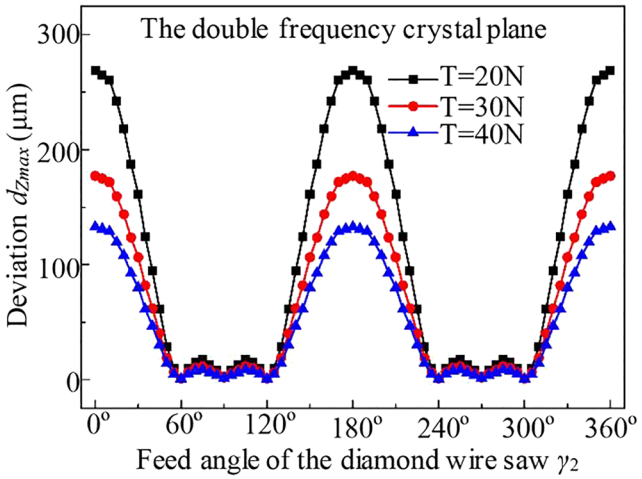

Fig. 21 Variations of d_{Zmax} with γ_2 for the double-frequency crystal plane

For the triple-frequency crystal plane, the E_d would have peak values while the feed angle of diamond wire saw has values of 30°, 150°, 210°, and 330°. While the feed angle is 90° or 270°, the corresponding E_d would be zero. At this time, the anisotropy would have no effect on the surface shape deviation.

4.2 Influence of γ on surface shape deviation

For the (001) crystal plane, material properties are symmetrical to the feed direction of the diamond wire saw, as analyzed in Section 4.1. So anisotropy has no effect on the surface shape deviation of the slice.

For the double-frequency crystal plane and the triple-frequency crystal plane, anisotropy would have an effect on the surface shape deviation of the slice. The influence rules of anisotropic properties of KDP crystal on the surface shape deviation of slice for the double-frequency crystal plane and the triple-frequency crystal plane are analyzed.

4.2.1 Influence of γ_2 on surface shape deviation for the double-frequency crystal plane

For the double-frequency crystal plane, variations of the maximum value of the surface shape deviation of slice d_{Zmax} with the cutting angle of the diamond wire saw γ_2 are shown in Fig. 21.

It can be seen from Fig. 21 that the change rule of d_{Zmax} with γ_2 is similar to that of E_d in Fig. 20. For the double-frequency crystal plane, the change rule of d_{Zmax} with γ_2 is as follows.

The d_{Zmax} has large values while γ_2 has values of 0° or 180°. At this time, the anisotropy of KDP crystal has the largest effect on the surface shape deviation. The d_{Zmax} would have small values close to zero, when the γ_2 is in the range of 60°–120° or 240°–300°. At this time, the anisotropy of KDP crystal would have a small effect on the surface shape deviation. It can also be observed that the d_{Zmax} would decrease with the increase of the tension force. While for a certain crystal plane, the change rule of the d_{Zmax} with the feed angle of the diamond wire saw is the same regardless of the other parameters, such as the size of KDP crystal and the tension force of the diamond wire saw.

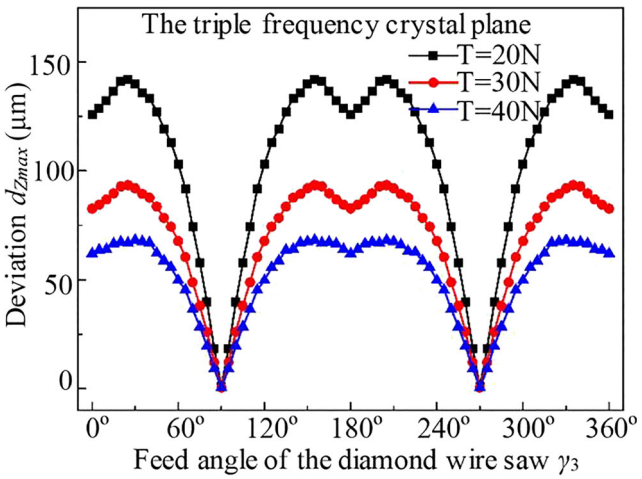

Fig. 22 Variations of d_{Zmax} with γ_3 for the triple-frequency crystal plane

4.2.2 Influence of γ_3 on the surface shape deviation for the triple-frequency crystal plane

For the triple-frequency crystal plane, variations of the maximum value of the surface shape deviation of slice d_{Zmax} with the cutting angle of the diamond wire saw γ_3 are shown in Fig. 22.

It can also be seen from Fig. 22 that the change rule of d_{Zmax} with γ_3 is similar to that of E_d in Fig. 20. For the triple-frequency crystal plane, the change rule of d_{Zmax} with γ_3 is as follows.

When γ_3 is about 30°, 150°, 210°, or 330°, the d_{Zmax} would have peak values. At this time, the anisotropy of KDP crystal has the largest effect on the surface shape deviation. The d_{Zmax} would be zero, when the γ_3 has values of 90° or 270°. At this time, the anisotropy of KDP crystal would have no effect on the surface shape deviation. It can also be observed that the d_{Zmax} decreases with the increase of tension force while the change rule of the d_{Zmax} with the γ_3 is the same regardless of the tension force.

5 Conclusion

In this paper, the anisotropy of KDP crystal in slicing by the diamond wire saw is analyzed through coordinate changes. A model of diamond wire saw considering the anisotropy of KDP crystal is established to obtain the sawing force. Then the effect of anisotropy on surface shape deviation of the slice is studied. Conclusions can be summarized as follows:

1 Distributions of elastic modulus in slicing of the (001) crystal plane, the double-frequency crystal plane, and the triple-frequency crystal plane are obtained. The difference of integration values of the elastic modulus at both sides of the feed direction is chosen to characterize the degree of influence of anisotropy on the surface shape deviation of slice.

2 In slicing of KDP crystal by the diamond wire saw, the sawing force is obtained by simulation while the anisotropic properties are considered. The surface shape deviation of slice is obtained by the sawing force. The effect of anisotropy of KDP crystal on surface shape deviation of slice is got.

3 For the (001) crystal plane, the anisotropic properties of KDP crystal have no effect on the surface shape

deviation of slice, regardless of the feed angle of the diamond wire saw.

4 For the double-frequency crystal plane, the anisotropic properties would affect the surface shape deviation of slice. The surface shape deviation of slice would have small values close to zero, when the feed angle of the diamond wire saw is in the range of 60°–120° and 240°–300°.

5 For the triple-frequency crystal plane, the anisotropic properties would affect the surface shape deviation of slice. While the feed angle of the diamond wire saw is 90° or 270°, the surface shape deviation of slice would have the smallest value.

Acknowledgements This work was supported by the National Natural Science Foundation of China (51575317) and the Key Research and Development Program of Shandong Province, China (2019JZZY020209, 2019GGX104007).

Authors' contributions Zongqiang Li contributed to the conception of the study.

Peiqi Ge contributed significantly to the analysis.

Wenbo Bi contributed to the manuscript preparation.

Long Li performed the data analyses and wrote the manuscript.

Chengyun Li helped perform the analysis with constructive discussions.

Data availability The data and materials supporting the results of this article are included within the article.

Code availability Not applicable.

Declarations

Ethical approval Not applicable.

Consent to participate Not applicable.

Consent to publish The authors declare that this work has not been submitted elsewhere for publication, in whole or in part, and all the authors listed have approved the manuscript that is enclosed.

Competing interests We declare that we have no financial and personal relationships with other people or organizations that can inappropriately influence our work. We have no competing financial interests.

References

1. Chen M, Pang Q, Wang J, Cheng K (2008) Analysis of 3D microtopography in machined KDP crystal surfaces based on fractal and wavelet methods. Int J Mach Tool Manu 48(7–8):905–913
2. Pritula I, Bezkrovnaya O, Lopin A, Kolybaeva M, Puzikov V, Zubatyuk R, Shishkin O, Gayvoronsky V (2013) Optical properties of KDP crystals doped with pyrenetetrasulfonic acid salt. J Phys Chem Solids 74(3):452–456
3. Ge M, Bi W, Ge P, Bi Y (2016) Experimental research on KDP crystal slicing with resin bonded diamond abrasive wire saw. Int J Adv Manuf Tech 87(5–8):1671–1676
4. Li Z, Ge P, Bi W, Liu T, Wang P, Gao Y (2018) Coupling stress caused by thermal and slicing force in KDP crystal slicing with fixed abrasive wire saw. Int J Adv Manuf Tech 96(9–12):4333–4343
5. Wu H (2016) Wire sawing technology: a state-of-the-art review precision engineering. Precis Eng 43:1–9
6. Fang T, Lambropoulos J (2002) Microhardness and indentation fracture of potassium dihydrogen phosphate (KDP). J Am Ceram Soc 85(1):174–178
7. Zhang Q, Liu D, Wang S, Zhang N, Mou X, Sun Y (2009) Mechanical parameters test and analysis for KDP crystal. J Syn Cryst 38(6):1313–1319 **(in Chinese)**
8. Guin C, Katrich M, Savinkov A, Shaskolskaya M (1980) Plastic strain and dislocation structure of the KDP group crystals. Krist Tech 1980, 15(4): 479–488
9. Chen H, Dai Y, Zheng Z, Gao H, Li X (2011) Effect of crystallographic orientation on cutting forces and surface finish in ductile cutting of KDP crystals. Mach Sci Technol 15(2):231–242
10. Yang S, Zhang L, Xie H, Liu W (2021) Interaction potential function for the deformation analysis of potassium dihydrogen phosphate using molecular dynamics simulation. Comput Mater Sci 187:110122
11. Clark W, Shih A, Hardin C, Lemaster R, Mcspadden S (2003) Fixed abrasive diamond wire machining-part I: process monitoring and wire tension force. Int J Mach Tool Manu 43(5):523–532
12. Clark W, Shih A, Lemaster R, Mcspadden S (2003) Fixed abrasive diamond wire machining-part II: experiment design and results. Int J Mach Tool Manu 43(5):533–542
13. Hardin C, Qu J, Shih A (2004) Fixed abrasive diamond wire saw slicing of single-crystal silicon carbide wafers. Mater Manuf Process 19(2):355–367
14. Li S, Zhang J, Wan B, Li Y (2012) The force theoretical analysis and experiment for wire saw with UVM cutting SiC monocrystal. Appl Mech Mater 117-119:1728–1735
15. Liu T, Ge P, Gao Y, Bi W (2017) Depth of cut for single abrasive and cutting force in resin bonded diamond wire sawing. Int J Adv Manuf Tech 88(5–8):1763–1773
16. Wang P, Ge P, Gao Y, Bi W (2017) Prediction of sawing force for single-crystal silicon carbide with fixed abrasive diamond wire saw. Mat Sci Semicon Proc 63:25–32
17. Huang H, Li X, Xu X (2017) An experimental research on the force and energy during the sapphire sawing using reciprocating electroplated diamond wire saw. J Manuf Sci Eng.-Trans ASME 139(12):121011
18. Sun Y (2012) Study on the mechanical properties and cracking phenomenon of KDP crystal. University of Shandong, Dissertation **(in Chinese)**
19. Bidiville A, Wasmer K, Michler J, Nasch P, Meer M, Ballif C (2010) Mechanisms of wafer sawing and impact on wafer properties. Prog Photovoltaics 18(8):563–572
20. Yang F, Kao I (2001) Free abrasive machining in slicing brittle materials with wiresaw. J Electron Packag 123:254–259
21. Li C, Li X, Wu Y, Zhang F, Huang H (2019) Deformation mechanism and force modelling of the grinding of YAG single crystals. Int J Mach Tool Manu 143:23–37
22. Li C, Wu Y, Li X, Ma L, Zhang F, Huang H (2020) Deformation characteristics and surface generation modelling of crack-free grinding of GGG single crystals. J Mater Process Tech 279:116577
23. Xie Y, Bhushan B (1996) Effects of particle size, polishing pad and contact pressure in free abrasive polishing. Wear 200(1):281–295
24. Williams J (2005) Engineering tribology. Cambridge: Cambridge University Press
25. Huang W, Yu D, Zhang X, Zhang M, Chen D (2018) Ductile-regime machining model for ultrasonic elliptical vibration cutting of brittle materials. J Manuf Process 36:68–76

26. Xiao X, Zheng K, Liao W, Meng H (2016) Study on cutting force model in ultrasonic vibration assisted side grinding of zirconia ceramics. Int J Mach Tools Manuf 104:58–67
27. Marshall D, Lawn B, Evans A (1982) Elastic/plastic indentation damage in ceramics: the lateral crack system. J Am Ceram Soc 65(11):561–566
28. Chung C, Le V (2015) Depth of cut per abrasive in fixed diamond wire sawing. Int J Adv Manuf Tech 80:1337–1346